Versão online: http://www.lneg.pt/iedt/unidades/16/paginas/26/30/95

Comunicações Geológicas

Comunicações Geológicas (2011) 98, 61-71
ISSN: 0873-948X; **e-ISSN:** 1647-581X

Imaging spectroscopy answers to acid mine drainage detection at S. Domingos, Iberian Pyrite Belt, Portugal

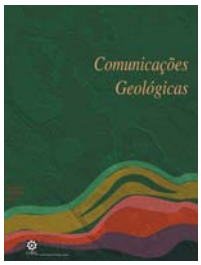

Respostas da espectroscopia de imagem na detecção da drenagem ácida mineira em S. Domingos, Faixa Piritosa Ibérica, Portugal

L. Quental[1*], A.J. Sousa[2], S. Marsh[3], G. Brito[4], M.M. Abreu[5]

Recebido em 27/06/2011 / Aceite em 15/09/2011
Disponível online em Outubro de 2011 / Publicado em Dezembro de 2011

Artigo original
Original article

Abstract: The application of Imaging Spectroscopy (IS) to Acid Mine Drainage (AMD) detection has been mostly based on specific mineralogical mapping from spectral libraries or on field spectra derived information. This work presents the mapping results obtained using field spectra and other mapping where a multi-source spectral methodology mapped the area in terms of high correlation of mineralogical assemblages related to low pH.
The case study is the S. Domingos Mine, a paradigmatic example of AMD due to long term exploration dating back to pre-roman times, where in modern times mining lasted for more than a century ceasing in 1966. Throughout the mine's lifetime the major mined elements varied from Cu, Au, Ag and Fe, to dominant Cu and S near the end.
The comparison of the two maps depicts the improvement given by a multi-source spectral methodology, by isolating copiapite (coquimbite) (alunite) as mineralogical assemblages of low pH at correlations above 0.9.

Keywords: AMD; waste field map; multi-source spectral methodology; low pH mineralogical correlation maps.

Resumo: A aplicação de imagens hiperespectrais ou de Espectroscopia de Imagem (EI) na detecção de Drenagem Ácida Mineira (DAM) tem sido fundamentalmente baseada em cartografia mineralógica utilizando bibliotecas mineralógicas espectrais ou em cartografia derivada de espectros de campo. Este trabalho apresenta a cartografia obtida utilizando medições espectrais de campo e compara com outra cartografia, onde uma metodologia utilizando espectros multifonte cartografa a área em termos de alta correlação de associações mineralógicas relacionadas com pH baixo.
O caso de estudo corresponde à Mina de S. Domingos, um exemplo paradigmático de DAM devido à longa exploração mineira com primórdios pré-romanos e com actividade por mais de um século até 1966. Durante a exploração da mina os elementos extraídos variaram desde o Cu, Au, Ag e Fe a dominantemente Cu e S no seu término.
A comparação entre as duas cartografias evidencia o refinamento obtido utilizando a metodologia espectral multifonte, pelo isolamento de associações mineralógicas copiapite (coquimbite) (alunite) de pH baixo com correlações acima de 0,9.

Palavras-chave: DAM; mapa de materiais mineiros; metodologia espectral multifonte; mapa de correlações mineralógicas de baixo pH.

[1]Laboratório Nacional de Energia e Geologia. Apartado 7586, 2611-901 Amadora. Phone: (+351) 214 705 400.
[2]CERENA, Instituto Superior Técnico, Universidade Técnica de Lisboa (TULisbon). Avenida Rovisco Pais, 1, 1049-001 Lisboa. Phone: (+351) 218417247
[3]British Geological Survey. Kingsley Dunham Centre, Keyworth, Nottingham NG12 5GG. Phone: +44 (0)115 936 3100.
[4]CICEGe, Faculdade de Ciências e Tecnologia, Universidade Nova de Lisboa. Quinta da Torre, 2829-516 Monte da Caparica. Phone: (+351) 21 2948349.
[5]UIQA, Instituto Superior de Agronomia, Universidade Técnica de Lisboa (TULisbon). Tapada da Ajuda 1349-017 Lisboa Phone: (+351) 213 653 199.
*Corresponding author / Autor correspondente: lidia.quental@lneg.pt

1. Introduction

Relying on the spectroscopy principles established in the XIX century (Schaepman *et al.*, 2006; 2009), the Imaging Spectroscopy (IS) expands the point concept of spectroscopy by gathering spatial data over large areas with high spectral resolution.

Within the broad range of images available in Earth Observation systems, IS or hyperspectral imaging is a particular type within the optical passive sensors. These images are characterized by many bands with very narrow bandwidths and with a variable signal to noise ratio (SNR), from relatively low, >60:1, in Hyperion spaceborne sensor (Kruse *et al.*, 2003), to high, >500:1, in HyMap™ airborne sensor (Cocks *et al.*, 1998). The mapping capabilities are then extended to a mineralogical and chemical level, providing an adequate tool to use on environmental concerns, e.g., in Acid Mine Drainage (AMD) issues and subsequent release of hazardous elements. The detection of AMD using IS has been addressed in several ways, being the dominant based on mineralogical assemblages, such as iron-bearing sulfates, oxides, and oxyhydroxides, which are identifiable through specific spectral ranges, due to their chemical and structural properties. Details on the basis for spectral interpretation and mineral identification are given in Clark (1999), Crowley *et al.* (2003) and Montero *et al.* (2005).

The assessment of AMD and consequent release of hazardous elements has been achieved based upon pH values of precipitation of minerals, assigning specific mineralogical assemblages of iron bearing minerals to pH ranges. Thus, increasing pH values were described in sequences of copiapite-jarosite-goethite-hematite, based on standard spectral libraries measured in laboratory (Clark *et al.*, 1993), or similarly pH related others, in Swayze *et al.* (1996; 2000); Dalton *et al.* (1998); Montero (2002) and Montero *et al.* (2005). Other works, e.g., Riaza *et al.* (2007) and Riaza & Mueller (2009), have monitored the AMD evolution using also field and laboratory spectroscopy. Another approach is given by Kemper & Sommer (2003) applied to an acid spill derived from a tailings dams´s failure. On this, field spectra of the contaminants were used to map the images, when properly correlated with chemical content of the sampled material.

A method was developed by Ong *et al.* (2003) where quantitative physiochemical maps from airborne IS are transferred from spectral prediction of pH from laboratory analysis. This ability has also been tested for monitoring

purposes, and Zabcic *et al.* (2005) demonstrated its usefulness in a distinct environment (the Iberian Pyrite Belt). Other more generic approaches encompass the generation of thematic maps of major mine tailings-related surface materials and indirect attribution of pH degrees, based on the correlation with the extent and degree of vegetation cover affected by tailings material (Richter *et al.*, 2008).

In this study two types of procedures for IS mapping are applied to the S. Domingos mining area, a paradigmatic example of AMD. One relies on the use of field spectra gathered contemporaneously with airborne IS data acquisition, and focused on specific AMD materials. The resultant waste mining material map is based on a full pixel algorithm of similarity measure using angular distances between the field and image spectra.

The other type of mapping is also based on the same type of algorithm but using instead, as input, multi-source spectral data correlated at multi-scale level on a wavelength basis. The objective is to minimize uncertainty of the results when using IS data. The two maps are compared highlighting the advantages of the latter when mapping AMD related areas, and its usefulness as a constituent part of an environmental assessment system.

2. Test site and data sets

2.1. S. Domingos mining area

S. Domingos is an old mine located in SE Portugal (Fig. 1) and contains a Volcanogenic Massive Sulphide deposit typical of the Iberian Pyrite Belt. The ore-body consists of a sub-vertical lens containing ≈25 Mt of sulphides (mostly pyrite), located on top of a Volcano-Sedimentary sequence (Volcano Sedimentary Complex) comprising black shales and different meta-volcanic rocks dated from Late Famennian to Late Visean (Matos, 2004; Matos & Martins, 2006; Mateus *et al.*, 2011). With long term mining exploration dating back from pre-roman times to modern times the elements exploited varied throughout the mine lifetime. While in the early times Cu, Au and Ag, with iron, were the dominant exploited metals, in the last nearly 100 years Cu and S dominated the mine products until its closure in 1966.

The area depicts a significant environmental footprint, the most prominent concern being related to AMD and subsequent release of hazardous elements on soils and waters. High contents of hazardous elements on soils, sediments and waste materials, can reach maximum values of As=15,900 mg kg−1, Pb=32,170 mg kg^{-1}, Hg=9300 mg kg^{-1}, Sb=5640 mg kg^{-1}, Zn=14,850 mg kg^{-1}, S=8 mg g^{-1} and Fe=400 mg g^{-1}, while pH measured is as low as 1.6 in Achada do Gamo (Tavares *et al.*, 2008).

These values are due both to the volume of ore exploited, ≈25 Mt, and to an inexistent or different environmental concept throughout its time of exploitation. $14.7x10^6$ m^3 of mining waste of several types are estimated to be present at S. Domingos, accumulated to thicknesses varying very irregularly from 14 m near the open pit to less than 1 m at the locations furthest downstream (Matos, 2004; Matos & Martins, 2006; Mateus *et al.*, 2011).

The development of several mining infrastructures, i.e., cementation tanks, sulphur factories, railway for the ore transportation and harbour (Fig. 1), facilitated the dispersion of waste mining materials, and pollutants enclosed, visible within an area of 50 km^2 (Quental *et al.*, 2003).

According to the Thornthwaite classification, the climate of the region is semiarid mesothermic, with no excess water and small thermal efficiency in the hot season, and it can be divided in two distinct seasons, a wet period from November to March and a dry period from May to September. The annual average air temperature is 17.6 ºC, and annual precipitation is 559 mm (Abreu *et al.*, 2008). These climatic characteristics control the cycling of metals and acid by the precipitation and dissolution of efflorescent salts, recognized as an important process at mine sites (Hammarstrom *et al.*, 2005).

Although some indicative and safety measures were undertaken by local authorities, informing about the danger and the installation of protective fences, no remediation measures have been applied to this area.

2.2. Data sets

2.2.1. Airborne data

Airborne IS data from HyMap™ sensor covered the S. Domingos mining area on 21st August 2000, containing the area depicted in Fig. 1. This whiskbroom sensor, owned by Hyvista Corporation (HVC), covers the spectral range 450 to 2500 nm with 126 bands, and spectral bandwidth varying between 10-20 nm (Cocks *et al.*, 1998). The ground instantaneous field of view (GIFOV) for these data is at maximum 4.3 m. HVC used a Dornier 228 aircraft operated by the Deutsches Zentrum für Luft und Raumfahrt (DLR) to acquire the data. The dataset was delivered by HVC as radiance and also calibrated to reflectance data (Quental *et al.*, 2003) using HyCorr software, which is a modified version of the ATmospheric REMoval (ATREM) (Gao *et al.*, 1999) software, with an Empirical Flat Field Optimal Reflectance Transformation™ (EFFORT) Polishing. The EFFORT as described by Goetz *et al.* (1997) and Boardman (1998) is an analytical process that bootstraps a linear adjustment to apparent reflectance spectra to improve the accuracy of spectra following calibration with ATREM.

The fligthlines were geocoded in UTM, WGS84 datum using Differential Global Positioning System (DGPS) flight data. An overview of the study area is given by the mosaiced fligthlines in Fig. 1.

The image processing was undertaken using the ENvironment for Visualizing Images (ENVI) software from ITT Visual Information Solutions (ITT, 2010).

2.2.2. Field spectral data

Field spectral data were gathered both to calibrate the images and to characterize the field materials. The spectra were collected across the area with an ASD FieldSpec@Pro spectrometer with wavelengths between 350-2500 nm, owned by the Bundesanstalt für Geowissenschaften und Rohstoffe (BGR) (Quental *et al.*, 2002a). The data was acquired in reflectance spectra in 100 milliseconds, with less than 10 nm spectral resolution. The collection was focused on selected targets depicted in Fig. 1 and named S. Domingos (SD), Tapada (TA); Achada do Gamo (AC); Telheiro (TE); Pomarão N (PN) and Pomarão S (PS). The criteria for selection encompass the diversity of geological features, mining aspects and environmental issues (Quental *et al.*, 2002a; 2002b). Thus, S. Domingos corresponds to the open pit with an ENE S. Domingos village, Achada do Gamo contains the sulphur factories and large volumes of waste materials, while Telheiro is located S of Achada do Gamo and contains downstream of S. Domingos acid river where converges a clean river, and Pomarão S is the place where the ore was shipped. Tapada and Pomarão N are reference areas not contaminated by the mining activity and considered background areas. Particular emphasis was given to supposedly contaminated targets, respectively S. Domingos, Achada do Gamo, Telheiro and Pomarão S. Based on the geochemical concentration of some of the targets (Quental *et al.*,

2002a; Tavares *et al.*, 2009), their field descriptions and spectral characteristics, 91 spectra were selected for this work.

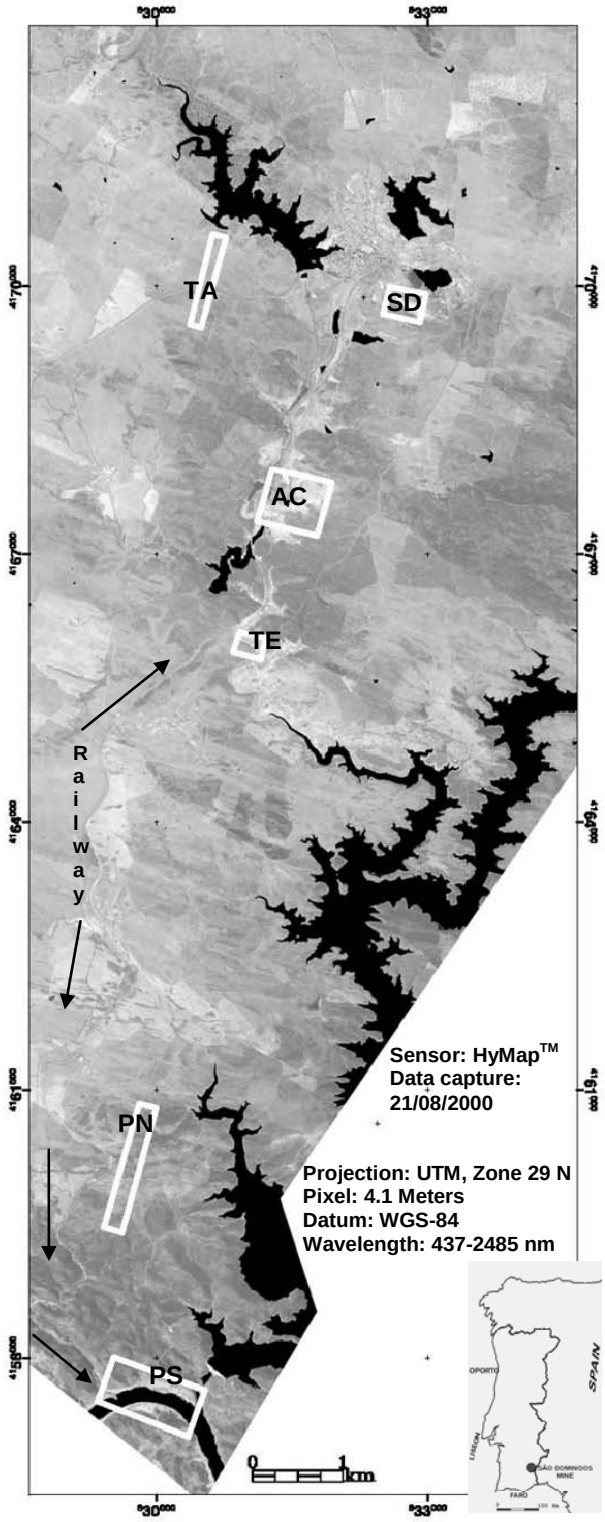

Fig. 1. Location of the mine site and sampling areas Tapada (TA), S. Domingos (SD), Achada do Gamo (AC), Telheiro (TE), Pomarão N (PN) and Pomarão (PS) (after Quental *et al.*, 2002a). Details are given in Section 2.2.2.

Fig. 1. Localização da mina e áreas de amostragem Tapada (TA), S. Domingos (SD), Achada do Gamo (AC), Telheiro (TE), Pomarão N (PN) e Pomarão (PS) (adapt. de Quental *et al.*, 2002a). Detalhes são dados na Secção 2.2.2.

2.2.3. Mineralogical spectral library

The minerals contained in the spectral library of United States Geological Survey (USGS) (Clark *et al.*, 2007), were measured on at least one of four different spectrometers. However, most of the spectra presented herein were derived from Clark *et al.* (1993) and were measured on a custom-modified, computer-controlled Beckman spectrometer at the USGS Denver Spectroscopy Lab. Wavelength accuracy is in the order of 0.5 nm in the near-IR and 0.2 nm in the visible.

The criteria for selection of the minerals were focused on iron minerals as indicators of variable degrees of AMD, and also others detected by X-Ray Diffraction (XRD) on clay fraction materials (Abreu *et al.*, 2001; Quental *et al.*, 2002a) on the study area. 70 minerals were selected, from which several correspond to variations of the same group (Table 1), e.g. in the case of Jarosite group some content on chemical elements, such as Pb (J8) or K (J6), among others, is distinguished.

Table 1. Minerals from the USGS spectral library (Clark *et al.*, 2007) presenting high correlations and with Correlation Matrix Name (CMN) adopted.

Tabela 1. Minerais da biblioteca espectral do USGS (Clark *et al.*, 2007) que apresentam altas correlações e com o Nome da Matriz de Correlação (NMC) adoptado.

USGS Spectral library filename	CMN	USGS Spectral library filename	CMN
Ammonioalunite NMNH145596	aA	Jarosite GDS100 Na-Sy 90C	J3
Ammonio-jarosite SCR-NHJ.	aJ	Jarosite GDS101 Na-Sy 200	J4
Ammonio-Smectite GDS86	aS	Jarosite GDS24 Na	J5
Alunite GDS84 Na03	A1	Jarosite JR2501 K	J6
Alunite GDS83 Na63	A2	Jarosite NMNH95074-1 Na	J7
Alunite GDS82 Na82	A3	Jarosite WS368 Pb	J8
Alunite AL706 Na	A4	Jarosite SJ-1 H3O - 10-20%	J9
Alunite HS295.3B	A5	Kaolinite CM9	K
Copiapite GDS21	Co	Kaolinite KGa-1 (wxyl)	K2
Coquimbite GDS22	Cq	Kaolinite KGa-2 (pxyl)	K3
Chlorite SMR-13.c 45-60um	C4	Kaolinite KL502 (pxyl)	K4
Chlorite SMR-13.d 30-45um	C5	Kaolinite GDS11 <63um	K5
Chlorite SMR-13.e <30um	C6	Kaolinite CM3	K6
Ferrihydrite GDS75	F	Kaolinite CM5	K7
Goeth. WS222	G1	Kaolinite CM7	K8
Goeth. HS36.3	G2	Illite GDS4	I1
Goethite WS219	G3	Illite IMt-1.a	I2
Goethite WS220	G4	Illite IMt-1.b <2um	I3
Hematite 2%+98%Qtz GDS76	H1	Illite IL101 (2M2)	I4
Hematite GDS27	H2	Illite IL105 (1Md)	I5
Hematite GDS69.a 150-250u	H3	Lepidocrosite GDS80 (Sy)	L
Hematite GDS69.b 104-150u	H4	Pyrite HS35.3	Py1
Hematite GDS69.c 60-104um	H5	Pyrite S142-1	Py2
Hematite GDS69.d 30-45um	H6	Pyrite S26-8	Py3
Hematite GDS69.e 20-30um	H7	Pyrite S29-4	Py4
Hematite GDS69.f 10-20um	H8	Pyrite S30	Py5
Hematite GDS69.g <10um	H9	GDS31 0-74um fr	Q2
Hematite HS45.3	Ha	Quartz HS32.4B	Q3
Hematite WS161	Hb	Quartz GDS74 Sand Ottawa	Q4
Hematite FE2602	Hc	Sulfur GDS94	S
Jarosite GDS99 K-y 200C	J1	Schwertmannite BZ93-1	Sc
Jarosite GDS98 K-Sy 90C	J2		

3. Methodology

The aim is to assess the AMD spatial pattern over the area, focusing on the acid generating capabilities of the materials based on its spectral characteristics. Two different methodologies were used encompassing field and image derived spectra. One of the methodologies uses also mineralogical information from standard spectral libraries (Clark *et al.*, 2007).

3.1. AMD waste materials mapping

The procedures developed for AMD waste material contamination mapping are summarized as follows into four main steps (Quental *et al.*, 2002a): I) analysis based solely on image information using spectral algorithms, II) selection of target area based on expert information, III) using field spectral data for classification and IV) enhancement of classified image. These procedures and their relationship are specified on the flow diagram of Fig. 2.

In I) a standard sequential procedure including Minimum Noise Fraction (MNF) transform (Boardman *et al.*, 1994) as modified from Green *et al.* (1988) and Pixel Purity Index (PPI) (Boardman *et al.*, 1995) was used. The endmembers retrieved on this analysis correspond to n=48 and were considered as reference spectra for the next step, using the Spectral Angle Mapper (SAM, Kruse *et al.*, 1993). This algorithm is a physically based spectral classification that uses an n-dimensional angle to match pixels to reference spectra, treating them as vectors in the space with dimensionality equal to the number of bands.

On part II), the analysis of SAM results shows that several classified areas are known to be non-contaminated or even affected by mining works. To facilitate the next processing steps, minimise the data set size and focus in the area of interest, the HyMap^{TM} data set 1 has been masked of these classified areas, including also strong vegetation signatures, leading to HyMap^{TM} data set 2.

On part III) a careful observation and analysis of spectroradiometric field signatures, which takes into account ancillary data, geochemical or mineralogical, when it exists, is involved. Even if some signatures are similar they have been also included, due to their importance and for eventual merging at the end. Others are not shown, once they are clipped at the final classification. On part IV) the results are enhanced based on the spectral, spatial and statistical analysis of each class, namely using a supervised classification Mahalanobis Distance Algorithm (Richards, 1999), a direction-sensitive distance classifier splitting or eliminating part of the classes otherwise not captured by the SAM used angular distance. This part also includes the comparison with other data type, such as waste field map, geochemical or mineralogical data, and as a validation component.

3.2. AMD mineralogical correlation mapping

The validation of the maps produced from IS data poses some challenges implying an approach different than those used on most of the classical validation or accuracy assessment techniques as described in Congalton & Green (2009). One of these challenges is that IS data may map the environment with greater accuracy than the one that can be obtained by field crews or maps produced by other methods than Remote Sensing (Jacquez *et al.*, 2002; Aspinall *et al.*, 2002; Foody, 2008). In order to minimise uncertainty related to IS mapping, further developments were undertaken. The methodology developed relies on the use of multi-source spectral data at multi-scale levels and the establishment of a quantitative link among them based on the wavelength values. It takes advantage of one of the IS data characteristics, where the adjacent bands are very highly correlated and this correlation tends to be higher than the spatial correlation (Zhang & Desai, 2000).

The first part of the methodology, I), establishes the correlation among multi-scale spectral data according to the wavelength values: a) image derived endmembers based on MNF and PPI as referred previously; b) field measurements and c) mineralogical library (Clark *et al.*, 2007). From these are selected high correlations above 0.9 among the three data type. On part II), the selected spectra of field and endmembers are each inputted to the SAM. The part III) assigns to each of the produced map the mineralogical assemblages gathered through the Pearson correlation matrix using the ANDAD software (Sousa & Sousa, 2000). The final map, on part IV, is the intersection of pixels of each of the maps according to the similar mineralogical assemblage's threshold at 0.9. The uncertainty is two-fold minimised, by using as input only correlations of mineralogical assemblages above 0.9 and by the final map as resultant of an intersection of two distinct types of spectra as input for the SAM algorithm.

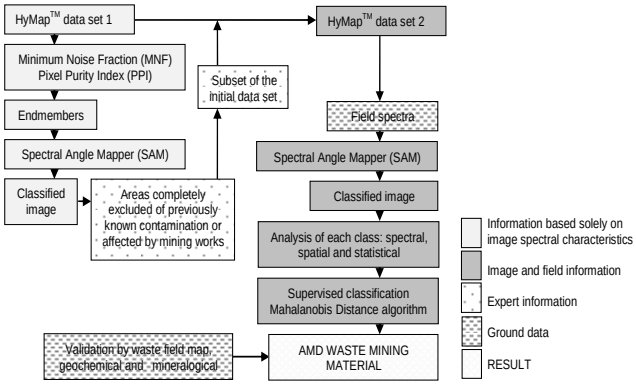

Fig. 2. Flow diagram of procedures for the AMD waste material mapping (adapted from Quental *et al.*, 2002a).

Fig. 2. Fluxograma de procedimentos para a cartografia de materiais mineiros (adapt. de Quental *et al.*, 2002a).

4. Results

4.1. AMD waste materials map

In Figure 3 the spatial pattern depicted by the spectral signatures of materials, from the surrounding area of the S. Domingos open pit to the Pomarão harbour are detailed. Southward from the Telheiro area (Fig. 1) the railway track used to transport the ore is highlighted by the dispersion of mining waste materials.

The most relevant field spectra used are compared in Fig. 4 with average results of equivalent image class. Further details of the characteristics of these classes concerning the distribution and a statistical parameter coefficient of variation (CV) are given in Table 2. The CV is the ratio of the standard deviation to the mean, and it is a useful statistic for comparing the degree of variation from one data series to another. Generally, a value of CV<1 indicates low data variability and probably the absence of anomalous data, which is verified in these classification results with an average CV of 0.29. The classes are also compared with other data type, namely waste field map, and mineralogy determined from XRD diffraction of soils clay fraction.

The most relevant class for the AMD detection is the mixed sulphur materials, classified as such due to visible native S within the samples measured. In fact, the total S content is commonly used in the prediction of acid production from mine wastes calculated in a static test of acid-base accounting (Levitan *et al.*, 2007). The total S content reaches values of 7.93 mg g^{-1} on waste materials sampled at Achada do Gamo, whilst the average values of 34 samples is 1.34 mg g^{-1} (Quental *et al.*, 2002a; Tavares *et al.*, 2008).

The designation contaminated on two of the classes reports to the fact that geochemical analysis of the materials measured

indicates high content of As, Hg, Pb, Sb and S (Tavares *et al.*, 2008; 2009). For both classes, the spectra were measured at Telheiro and values (mg kg^{-1}) have as maximum and mean respectively: As=15.90, 17.27; Hg=420.00, 29.32; Pb=73.15,10.65; Sb=2400.00, 236.12 and S (on mg g^{-1})=2.81, 0.62.

4.2. AMD correlation minerals map

The dataset for the Pearson correlation matrix is n=251, containing 70 USGS minerals (Clark *et al.*, 2007), 91 ASD field spectra and 90 endmembers. 118 bands were used encompassing the wavelengths intervals 434-1324 nm, 1448-1970 nm and 1989-2454 nm. From the output of the matrix are excluded the spectra which correlation with minerals are <0.9, as well as the ones not containing any environmental indicator related to AMD, i.e., only quartz, a-smectite, illite, kaolinite or alunite. With these criteria the ASD data were reduced to 57 field spectra and the endmembers to 36. Table 1 shows the minerals of the Clark *et al.* (2007) spectral library captured by the next step of the SAM and excluded the ones containing less than 30 pixels.

Tables 3 and 4 show the spectra correlations above 0.8 for the field spectra and endmembers. From these the minerals assemblages containing Co and or Cq at correlation ≥0.9 are detailed, sometimes isolated at this correlation level or already together with A, or at a lower correlation level with I, K or aS. Lower values of correlation, i.e., <0.8 do not depict different minerals except below 0.5 such as Q, a-jarosite (an exception to this is for AC-203, at 0.7) or Py. This indicates the significance of these mineralogical assemblages by isolation at high correlation level.

Table 2. Waste material´s classification results and characteristics of ancillary data on the classes.

Tabela 2. Resultados da classificação de materiais mineiros e características de dados auxiliares das classes.

Other data / Classes ($_{CV=}\frac{\sigma}{aver}$)	Main characteristics validated by partial field checking	Main field waste map units*	Mineralogical results XRD (soil clay fraction and salts) **	Classified areas (2,172,776,4 of 7,446,191.2m²)
Mixed sulphur materials (0.37)	High acidic potential, systematically maps surrounding tailings ponds and dams, highligths other unknown areas	Sulphidic ore, tailings (including black mud), dump leach piles, metallurgical slag	Jarosite, goethite, complex hydrated sulphates of Pb, Cu, Zn, K, Al, As, Fe and Ca, mixtures of copiapite and rumerite (vestigial)	83,243,116 (3.83%)
Metallurgical slag and leached rock (0.37)	Metallurgical slags and leached rocks, a generic class with large cover	Metallurgical slag, Dump leach piles and bleached and leached bedrock	Complex mixtures	570,027,072 (26.23%)
Fine material associated to metallurgical slag (0.62)	Essentially related to metallurgical slag, surrounding or overlaying some piles of these materials	Metallurgical slag, bleached and leached bedrock	Complex mixtures	19,818,969 (0.91%)
Yellowish ferricrete (0.22)	Significant spread in the area, particularly associated to areas affected by AMD	Tailings (including black mud), dump leach piles, leached and bleached rocks	Goethite, heamatite	246,955,698 (11.37%)
Reddish ferricrete (0.23)	Gossanous materials around open pit and other areas	Gossanous rock, goethite/heamatite bodies	Heamatite, goethite	44,176,678 (2.03%)
Mixed leached fragment rocks (0.34)	Heterogeneous materials of several grain sizes and colours	Dump leach piles, Metallurgical slag	Illite, kaolinite, quartzo	159,459,652 (6.76%)
Whitish leached rock (0.19)	Variation from previous, mostly located at higher altitude.	Bleached and leached bedrock, Dump leach piles	Illite, jarosite, interstratified vermiculite-smectite, goethite, quartz	146,784,913 (0.23%)
Red rock dump (0.14)	Particularly distributed around open pit area	Gossanous rock, undifferentiated waste rocks	Hematite, goethite	5,059,810 (7.35%)
Contaminated soils and sediments (0.24)	Spread over the area, including the village and part of dump leach piles, correspond to contaminated field spectra signature	White to yellow sedimentary deposits, Kaolinitic schist, Dump leach piles, kaolinitic schist	Kaolinite, illite, jarosite, natrojarosite, sulphur (vestigial)	876,322,067 (40.33%)
Contaminated soils with shale fragments (0.24)	A variation from the previous, with a more heterogeneous grain size and less dispersed	Bleached and leached rocks, Dump leach piles	Illite, kaolinite, quartz, jarosite	20,928,449 (0.96%)

* (Cottard, 2001) **(Abreu et al., 2001)

Table 3. Spectra correlations depicting the minerals with CMN adopted in Table 1.

Tabela 3. Correlações de espectros apresentando os minerais com a nomenclatura NMC adoptada na Tabela 1.

ASD Field Spec Pro		
n=57	≥0.9	0.8≤N≤0.9
TE-67	J(2-3-6-8) Sc	G(1-3-4) H1 I5 J(1-4-5-7-9) L Q(3-4)
TE-71	J(2-3-9)	G3 J(a-1-4-6-7-8) L Sc
TE-84	H1 J(2-3-8) Sc	G(1-3-4) H(a-2) I5 J(4-6-7-9) L Q(3-4)
TE-85	H1 Sc J(3-6-8) Q4 J6	F G(1-3-4) H(a-2) I5 J(2-4-5-7-9) L Q(2-3)
TE-90	G(3-4) J(2-3-6-7-8) L Sc	F G1 H(1-2) I(1-5) J (1-4-5-9) Q4
TE-92	J(2-3-6-8-9) L Sc	F G(1-3-4) H1 I1 J(a-1-4-5-7)
PN-97	F G(3-4) H1 J8 L Sc	G1 H(a-c-2) I(1-5) J(2-3-4-5-6-7-9) Q(3-4)
PN-98	G(3-4) H1 J8 L Sc	F G1 H(a-c-2) I(1-5) J(2-3-4-5-6-7-9) Q(3-4)
PN-99	G(3-4) J8 L Sc	F G1 H(a-1-2) I(1-5) J(2-3-4-5-6-7-9) Q(3-4)
PN-100	G3 L Sc	F G(1-4) H(1-2) I(1-5) J(2-3-6-7-8-9) Q(1-4)
PN-103	F G(1-3-4) H(1-2) I5 J(7-8) L Q4 Sc	C(1-5-6) H(a-b-c-3-7-8-9) I1 J(3-4-5-6) Py2 Q(2-3)
PN-105	G (1-3-4) H(1-2) I5 J8 L Q4 Sc	C6 F H(a-b-c-9) I1 J(2-3-4-5-6-7) Py2 Q(2-3)
PN-106	G(1-3-4) H(1-2) I5 J8 L Q4 Sc	C6 F H(a-b-c-9) I1 J(3-4-5-6-7) Py2 Q(2-3)
PN-107	G(3-4) H1 J8 L Q4 Sc	F G1 H(a-b-c-2) I(1-5) J(2-3-5-6-7) Q(2-3)
PN-111	Sc	F G(1-3-4) H(a-1) I1 J(2-3-6-7-8-9) L Q(1-4)
PN-112	Sc	F G(1-3-4) H(1-2) I(1-5) J(2-3-4-5-6-7-8-9) L Q(1-4)
PS-137	F G(1-3-4) H(1-2) I5 J(6-7-8) L Q4 Sc	C6 H(a-b-c-9) I1 J(2-3-4-5-9) Py2 Q(2-3)
PS-138	J(a-2-3-9)	J(1-4-6) L Sc
PS-143	J(2-3-6-8) Sc	F G(1-3-4) H1 I(1-5) J(1-4-5-7-9) L Q4
PS-146	J(2-3-9) Sc	G(3-4) H1 I1 J(a-1-4-5-6-7-8) L
PS-147	J(2-9)	J(a-1-3-4-6) Sc
PS-149	A3 Co	A(a-1-4-5-6) aS Cq I(a-4) K(3-8)
PS-151	A3 Co	A(a-1-2-4-5-6) aS Cq I(a-4) K8
PS-152	A(1-3-5) Co	A(a-2-4-6) aS Cq I(a-4) K(2-3-4-5-6-7-8)
PS-154	A(1-3-5) Co Cq	A(a-2-4-6)aS I(a-4) K(2-3-4-6-7-8)
PS-155	A(1-3-5) al Co Cq	A(a-2-4-6) aS I4 K(3-4-6-7-8)
PS-156	A(1-3-5) Co Cq	A(a-2-4-6) aS I(a-4) K(2-3-4-5-6-7-8)
PS-157	J(2-3-6-9)	G3 J(a-1-4-5-7-8) L Sc
PS-158	J(2-3-4-6-8) Sc	G(1-3-4) H1 I5 J(1-5-7-9) L Q(3-4)
PS-163	G3 J8 L Sc	F G(1-4) H(1-2) I(1-5) J(2-3-4-5-6-7-9) Q4
PS-164	J8 Sc	G(1-3-4) H1 I1 J(2-3-4-5-6-7-9) L Q(3-4)
PS-165	J8 Sc	G(1-3-4) H(a-1) I1 J(2-3-4-6-7-9) L Q(3-4)
PS-166	J8 Sc	F G(1-3-4) H1 I(1-5) J(1-2-3-4-5-6-7-9) L Q(3-4)
PN-169	Sc	F G(1-3-4) H(a-1-2) I(1-5) J(2-3-6-7-8-9) L Q(1-3-4)
PN-171	G(3-4) H1 J8 L Sc	C6 F G1 H(a-2) I(1-5) J(2-3-4-5-6-7) Q(2-3-4)
PN-172	Sc	G(3-4) H(a-1) J(2-8) L Q(1-4)
PN-174	C6 F G(1-3-4) H(1-2) I5 J(7-8) L Py2 Q(2-3-4) Sc	C(1-3-4-5) H(b-c-7-8-9) I1 J(4-5-6) Py(4-5)
PN-175	J8 F G(1-3-4) I(1-5) J(5-6-7) L Sc	C(1-4-5-6) H(b-1-2) J(2-3-4) Py2 Q(2-3-4)
PN-176	F G(1-3-4) H(1-2) I5 J8 L Q(2-3-4) Sc	C6 H(a-b-c-3-8-9) I1 J(6-7)Py2
TE_181	J(2-3)	H1 J(a-6-8-9) L Sc
TE_182	J2 Sc	G3 H(a-1) J(3-6-8-9) L Q4
TE_183	J(2-3-8) Sc	G(3-4) H(a-1) J(4-6-7-9) L Q(3-4)
TE_191	J3	H1 J(a-2-4-6-8-9) L Q(3-4) Sc
TE_192	J(2-3)	J(a-1-4-6-8-9) Sc
AC-203	Co	A(a-3) aS K(3-8)
AC-206	Co	A(a-1-3) aS K8
SD-210	F G(1-3-4) H(b-c-1-2-9) I5 J(7-8) L Py2 Q(2-4) Sc	C6 H(a-3-4-6-7-8) I1 J(2-3-4-5-6) Py5 Q3
SD-212	F G(1-3-4) H(c-1-2) I5 J8 L Q4 Sc	C6 H(a-b-3-7-8-9) I1 J(2-3-4-5-6-7-9) Py2 Q(2-3)
SD-215	H1 Q4 Sc	F G(1-3-4) H(a-b-c-2) I(1-5) J(3-6-7-8) L Q(2-3)
SD-216	Sc	F G(3-4) I1 J(2-9) L Q1
SD-217	G4 H1 Q4 Sc	F G(1-3) H(a-2) I(1-5) J(2-3-6-7-8) L Q3
SD-218	H1 Q4 Sc	F G(1-3-4) H(a-c-2) I(1-5) J(2-3-6-7-8) L Q(1-3)
SD-226	G4 Sc	F G(1-3) H(a-b-c-1-2) I(1-5) J(6-7-8) L Q(3-4)
SD-236	Sc	F G(1-3-4) H(a-1-2) I1 J(2-3-6-8-9) L Q(1-4)
SD-237	J8 G(1-3-4) H1 J6 L Q(3-4) Sc	F H(a-b-c-2) I(1-5) J(2-3-4-5-7-9) Py2 Q2
SD-246	F G(1-3) H(c-1-2) I5 J(7-8) L Q4 Sc	C6 H(b-3-7-8-9) I1 J(2-3-4-5-6-9) Py2 Q(2-3)
SD-248	F G(1-3-4) H(c-1-2) I5 J(7-8) L Q4 Sc	C6 H(a-b-3-7-8-9) I1 J(2-3-4-5-6-9) Py2 Q(2-3)

By contrast high correlations of J are generally accompanied at lower but similar correlation levels, by minerals that indicate some information concerning pH values, higher, such as G, Sc or L.

The intermediate field spectra and endmembers maps are intersected on a pixel basis according to the mineralogical assemblages of high correlation. The final map is depicted in Fig. 5. Details of both input spectra map, i.e., field and endmembers and the areas classified are given in Table 5.

The assemblages of copiapite-coquimbite minerals are usually considered as typical of environments with pH ≤ 3. The presence of these efflorescent salts has been reported at this test site, at Achada do Gamo (Fig. 1), during the dry summer season (Abreu *et al.*, 2010), and also in a similar environment within Iberian Pyrite Belt, typical of the banks of the stream affected by AMD (Ferreira da Silva *et al.*, 2009).

Other type of information, such as the one reported in PS-164 to PS-166 field spectra (Table 3) indicate a correlation ≥ 0.9 with J8 (Table 1) and Sc revealing the capture of hazardous elements like Pb, as described in field data in Silva & Figueiredo (2010). Although depicted at this correlation level, this class is not isolated at the threshold ≥ 0.9 for the endmembers mapping and thus not intersected in the final classes following this methodology.

The SAM results for each of the input spectra are depicted in Table 5, excluding broad classes with a higher dispersion such as schwertmannite, while other identical minor mineralogical assemblages are not intersected by both maps.

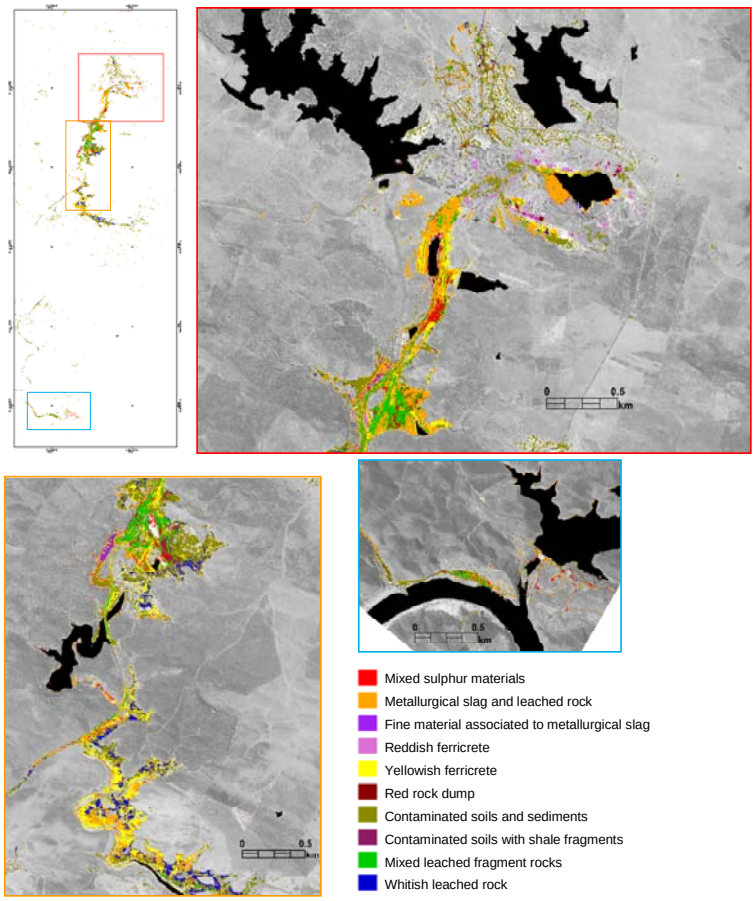

Fig. 3. Map of AMD waste materials (adapted after Quental & Brito, 2002c) based on field spectra and using SAM. Upper left: scheme of the detailed maps.

Fig. 3. Mapa de DAM de materiais mineiros (adapt. de Quental & Brito, 2002c) baseado em espectros de campo e utilizando o MAE. Campo superior esquerdo: esquema dos mapas detalhados.

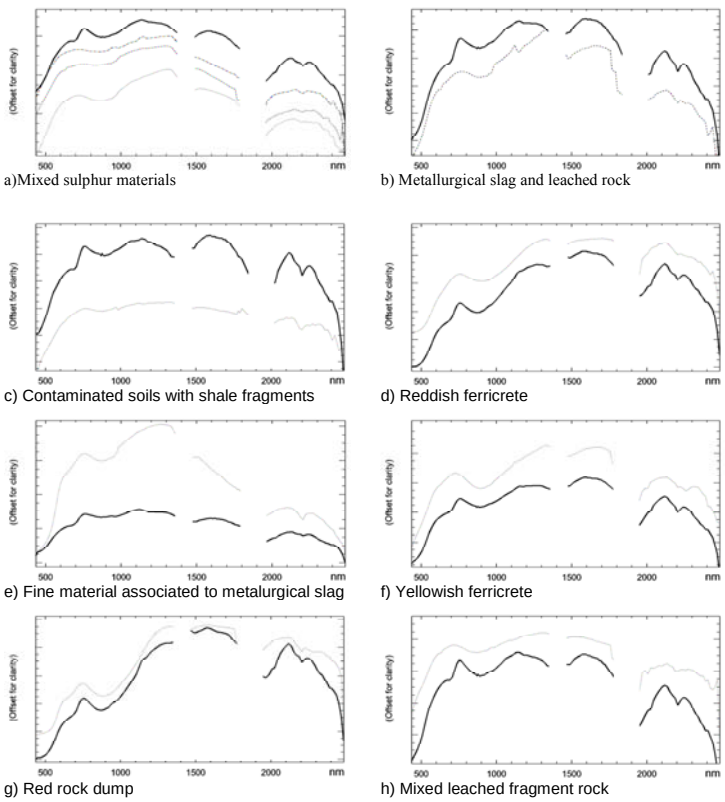

Fig. 4. Examples of most important average spectra of the HyMap™ classification image waste materials (solid dark line) and respective field spectra (dotted ligth).

Fig. 4. Exemplos dos espectros médios da classificação dos materiais mineiros mais importantes na imagem HyMap™ (linha sólida escura) e dos respectivos espectros de campo (ponteado claro).

Table 4. Correlation coefficients of endmember spectra used expressed in USGS spectral library minerals (Clark *et al.*, 2007), following CMN nomenclature of Table 1.

Tabela 4. Coeficientes de correlação dos espectros de termos extremos utilizados expressos em minerais da biblioteca espectral do USGS (Clark *et al.*, 2007), seguindo a nomenclatura do NMC da Tabela 1.

Hycorr-EFFORT mosaic endmembers		
n=36	≥0.9	0.80≤N≤0.9
6	J(2-9) Sc	G(3-4) H1 J(3-6-8) L
9	H1 J8 Q4 Sc	F G(1-3-4) H(a-2) I5 J(2-3-6) L Q(2-3)
11	H1 J8 Q4 Sc	F G(1-3-4) H(a-b-c-2) I5 J(2-3-6-7) L Q(2-3)
12	A(1-5) Co	A(2-3-6) Cq I(a-4)
13	Sc	F G(1-3-4) H(1-2) I1 J(2-3-6-7-8-9) L Q4
19	G(3-4) J(2-8) L Sc	F G1 H(1-2) I(1-5) J(3-4-5-6-7-9) Q4
22	G(1-4) H(b-c-1-2) I5 J8 Q(2-3-4) Sc	C6 F G3 H(a-3-7-8-9) J(6-7) L Py2
23	I1 Sc	F G(3-4) J(6-7-8) L
24	H(a-1) I5 J8 Q(2-3-4) Sc	F G(1-3-4) H(b-c-9-2) J6 L Py2
25	H(a-1) Q(3-4) Sc	F G(1-3-4) H(b-c-2-9) I5 J8 L Py2 Q2
29	G(1-3-4) H(1-2) I5 J8 L Q4 Sc	C6 F H(a-b-c-3-8-9) I1 J(2-3-6-7) Py2 Q(2-3)
35	Sc	F G(1-3-4) H1 I1 J(2-3-6-8-9) L
36	Sc	F G(1-3-4) H1 I1 J(2-3-4-6-7-8-9) L Q(3-4)
39	G3 J(2-9) L Sc	F G(1-4) H1 I1 J(3-4-6-7-8)
41	H(a-1) Q4 Sc	G(1-3-4) H(b-c-2) I5 J(2-3-6-8) L Q(2-3)
44	H1 J8 Q(3-4) Sc	F G(1-3-4) H(a-b-2) I5 J(2-3-6-7) L Q(2-3)
54	A(1-3) Co	A(a-2-4-5-6) aS Cq I(a-4) K(1-2-3-4-5-6-7-8)
56	L Sc	F G(1-4) H(1-2) I1 J(2-3-4-6-7-8-9) Q4
60	F G(1-3-4) H(b-c-1-2-9) I5 J8 L Q4 Sc	C6 H(3-4-6-7-8) I1 J(5-6-7) Py(2-5) Q(2-3)
64	J2 Sc	G(3-4) H1 J(a-3-4-6-7-8-9) L
65	H(a-1)	G(3-4) J8 L Q(3-4) Sc
66	I1 Sc	F G(1-3-4) H(1-2) I5 J(2-6-7-8) L Q4
68	Sc	F G(1-3-4) H(a-1-2) I(1-5) J(2-3-6-8) L Q(3-4)
70	H1 Q4 Sc	G(1-3-4) H(a-2)I5 J(2-3-6-8) L Q3
72	G(3-4) L Sc	G(1-3-4) H(a-2)I5 J(2-3-6-8) L Q3
73	F G(1-3-4) H2 J(6-7-8) L Sc	C6 H(b-c-1-9) I(1-5) J(2-3-4-5-9) Py2 Q4
75	J(2-9)	G3 J(a-3) L Sc
79	G(1-3-4) H(b-1-2) I5 J8 L Q(3-4) Sc	C6 F H(a-c-3-8-9) I1 J(2-3-6-7) Py2 Q2
85	A(1-3-5) Co	A(a-2-4-6) aS Cq I(a-4) K(2-3-4-6-7-8)
86	G(1-4) H(1-2) I5 J8 Q(3-4) Sc	C6 F G3 H(a-b-c-8-9) I1 J(3-6-7) L Py2 Q2
91	Sc	F G(1-3-4) H1 I1 J(2-3-6-7-8-9) L Q4
94	Co	A(a-1-3-5-6) aS I4 K(3-8)
101	Sc	F G(1-3-4) H(a-1) I1 J(2-3-6-7-8-9 L Q(3-4)
111	F G(3-4) I1 J7 L Sc	C6 G1 H(1-2) I5 J(2-3-4-5-6-8-9)
114	F G(1-3-4) H2 J8 L Sc	H(b-c-1-9) I(1-5) J(2-3-4-5-6-7-9) Py2 Q4
115	G(1-3-4) H(1-2) I5 J8 L Q4 Sc	C6 F H(a-b-c-8-9) I1 J(2-3-6-7) Py2 Q(2-3)

The class copiapite (coquimbite) (alunite) occurs near the open pit close to finely crushed sulphide ore and downwards following the railway line and surrounding acidic dams, and on areas of more acidic wastes such as sulphide piles and cementation tanks N of Achada do Gamo. Downstream of Telheiro, this class follows the S. Domingos river and borders the stream until the Chança river. Similarly this also occurs at the Pomarão harbour. This pattern is spatially related to the jarosite class, when not isolated on some areas. The class goethite-jarosite-lepidocrocite-schwertmannite (G-J-L-Sc) is mainly spread over the village, possibly indicating a more heterogeneous conditions of precipitation and mixtures of materials by remobilization, whilst the class goethite-lepidocrocite-schwertmannite (G-L-Sc) appears N of the open pit apparently more stable with iron secondary minerals at higher pH environment, possibly connected to the geological framework. This northern part of the open pit is occupied by gossan materials, metavolcanic rocks and shale piles (Matos, 2004).

As expected, there is a slight improvement on the CV on the final intersection map (Table 5). The area is significantly reduced on most of the classes when intersected, improving the accuracy of the results. Comparing the areas, the map derived from ASD field spectra are generically broadest, whilst the one derived from endmembers are smallest. This is most probably due to the lowest identifying capabilities at smallest image scales, but not excluding also the effect of the algorithm used for the endmembers extraction as well as previous steps in image processing chain.

Table 5. Details of multi-source spectral methodology individual maps and end results.

Tabela 5. Detalhes da metodologia multifonte nos mapas individuais e resultados finais.

MAPS / CLASSES	ASD FIELD			ENDMEMBERS			MINERALOGICAL CORRELATION ≥0.90		
	Spectra	Area (m²)	CV	Spectra	Área (m²)	CV	Spectra	Área (m²)	CV
Copiapite (Coquimbite) (Alunite)	149-151-152 154-155-203-206	108,996.04	0.22	#(12-85 54-94)	102,759.53	0.30	Intersection of correlation minerals	78,368.22	0.22
Jarosite	138-147-157-181	1,015,828.25	0.23	#(75)	24,004.68	0.22		7,127.44	0.20
Goethite-Jarosite-Lepidocrocite-Schwertmannite (G-J-L-Sc)	90-99-163	466,830.49	0.18	# (19-39)	15,263.48	0.16		7,648.55	0.15
Goethite-Lepidocrocite-Schwertmannite (G-L-Sc)	100	804,543.37	0.18	# (72)	2,723.22	0.12		1,798.67	0.12
SUM		2396,198.14			144,750.90			94,942.88	

5. Discussion

The issues related to validation in IS data as aforementioned, are particularly relevant when the result of a thematic map is mineralogical and chemical information, or indirectly related land cover classes such as the AMD waste materials map referred. The assessment of the waste material AMD map produced has been crossed with other data type showing coherent results (Table 2) and also the comparison of the areal extent of spectral classes to a point spectrum (Fig. 4). This relative assessment of the results does not take into account the locations at which class labels have been assigned, due to the fact that the point collection may not be representative of the pixel even if it looks at such by the human vision. This type of measure is not independent of the image processing system, thus not as an adequate accuracy assessment should be (Congalton, 2005).

The AMD waste mining materials classification generally matches well and gives coherent results when compared to field mapping and XRD analysis (Table 2) as well with geochemical data, when available (Quental *et al.*, 2002a; Tavares *et al.*, 2008; 2009). In the case of waste field map, the IS mapping provides much higher discrimination than the units defined, and the scale is not as accurate as the classification image. Ancillary data, such as geochemical results of soils in sampling points give an extensive intersection table of elements and confirm the pollutant content of the classes with high S, As, Fe, Cd, Pb and Hg contents, in the case of "contaminated soils and sediments" and "contaminated soils with shale fragments".

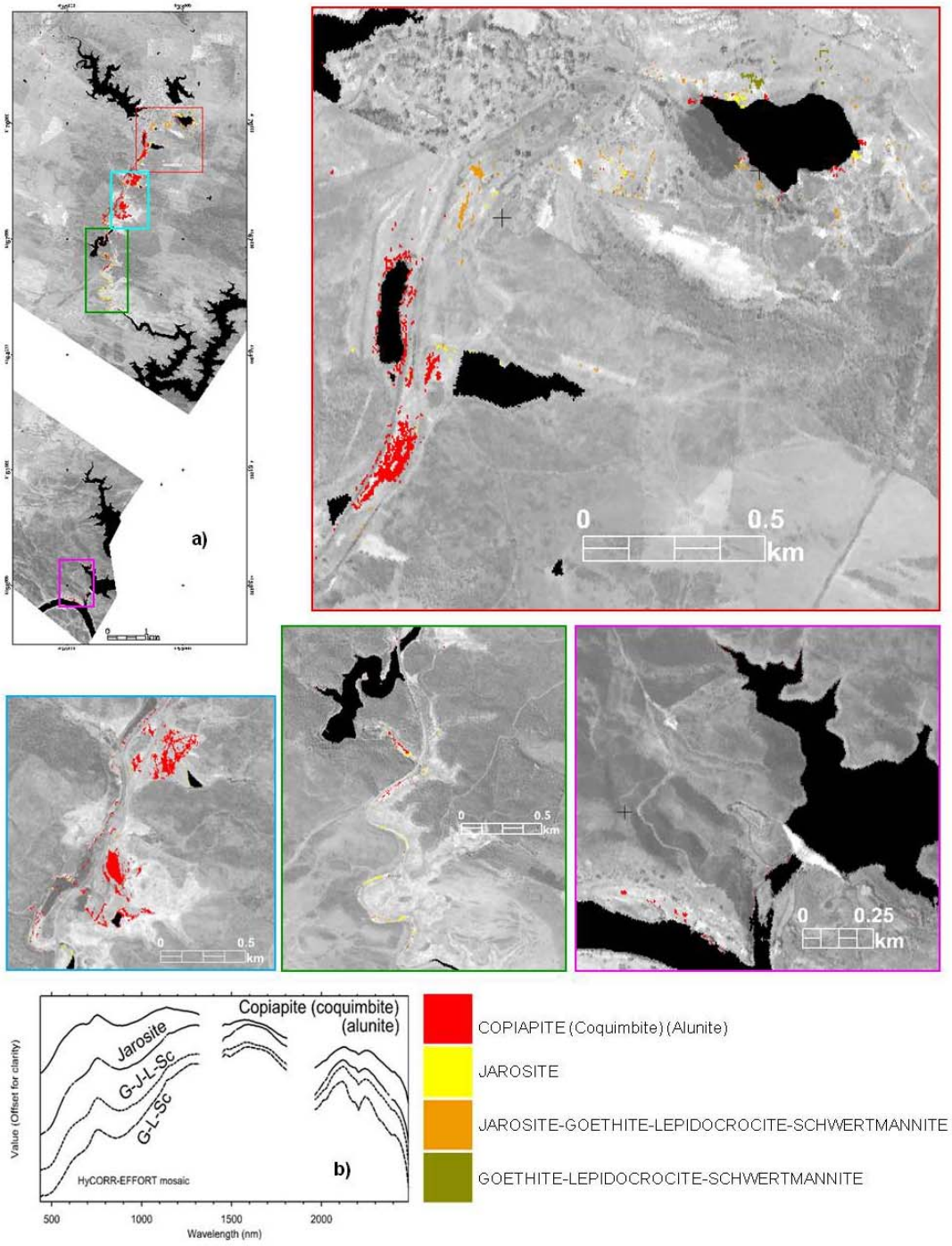

Fig. 5. a) Mineralogical correlation map ≥0.9 related to AMD. Assemblages of copiapite-coquimbite are typical of pH <3. Upper left: scheme of the detailed maps; b) Average values of spectra of the classes, lower left.

Fig. 5. a) Mapa de correlação mineralógica ≥0.9 associado à DAM. Associações de copiapite-coquimbite são típicas de pH <3. Campo superior esquerdo: esquema dos mapas detalhados; b) Valores médios dos espectros das classes, campo inferior esquerdo.

The spectral field signatures compared with average class as depicted in Fig. 4 or values of coefficient of variation (CV, Table 2) well below the threshold to designate homogeneous classes (CV<1 means: the distribution has low data variability and probably absence of anomalous data) are good indicators of similarity between distinct spectral data. However, the IS high spectral resolution data, may appear with a wide variability within apparently similar and nearby sampling points as detected on field spectra. This is confirmed by the multi-source spectral mapping (Fig. 5, Table 5), where the assignment of mineralogical spectra to unknown field spectra allows the establishment of correlation levels for the retrieval of information with improved knowledge and precision about the spectra considered. As an example, on the waste materials map, the spectrum PS=153,

collected on the same type of materials as PS=150 to PS=156, is included on the class "mixed sulphur materials" but not considered in Table 3, due to <0.8 correlation. This kind of information is advantageous, when correlating field and mineralogical library spectra based on wavelength values. In fact, the high precision information derived from spectral data requires a different type of approach and the establishment of a quantitative link works well to retrieve information of the spectra otherwise impossible just by visual analysis of absorption features and form (Fig. 4). The same quantitative link of correlation has been established for spectral data collected in 2007 at the same test site, and supports the conclusion that similar materials depict different spectral response and also that a low pH signature is spectrally isolated (Quental *et al.*, 2011).

Given the variability of similar spectra when quantitatively linked, some caution has to be taken when extending the spectra "contaminated soils and sediments", from geochemical content of the samples, to the image scale. Although pollutant content is assigned to the spectra based on geochemical content of the sampled material, the extrapolation to a wide area remains with a certain degree of uncertainty. Particularly in this case, subtle differences on the chemical composition might not be detected or differentiated using a SAM algorithm. To reliably check the extension of contamination spectral signatures, further local chemical and mineralogical analysis should be carried out, in places where there is no data available.

The waste materials map has another issue concerning the AMD potential that is not hierarchically defined to other classes than "mixed sulphur materials", representing this one the lowest value of the wastes pH. However, the next upper degree of the pH is difficult to assign to another class (Table 2). Although the AMD waste materials map depicts a global land cover with detailed "chemical" information related to the mining framework, it lacks quantitative information concerning the input field spectra or when exists reports to a different data type such as chemical or XRD analysis. By contrast the mineralogical correlation map ≥ 0.9 AMD minimizes the uncertainty by establishing a quantitative link using multi-source spectral data at different scales, i.e., laboratory, field and image. This quantitative link depicts mineralogical information to unknown field spectra and allows also the selection of very high correlations focusing on AMD specific mineralogical associations. In this case this knowledge isolates spectrally minerals related to very low pH environment (≤ 3), i.e., copiapite and or coquimbite. Another way to minimize the uncertainty of the mapping algorithm is to use different input spectra, i.e., from field measurements and image derived endmembers and selecting only the intersecting pixels of both maps.

Comparing the information derived from field spectra and endmembers the area mapped is larger in the former (Table 5). The smaller area covered by the endmembers may be due to the lowest identifying capabilities at smallest image scale, the most probable, but not excluding also the effect of the type of algorithm used for the endmembers extraction as well as previous steps on image processing chain.

The best mapping was obtained using some local spectral signatures in the Pomarão S, S. Domingos and Telheiro areas (Fig. 1), while signatures obtained directly in Achada do Gamo were less relevant. An explanation could be due to the complex chemical system that is present in Achada do Gamo with intense interactions of materials, while in Pomarão S they correspond to less abundant and mixed materials.

6. Conclusions

IS has many advantages when compared with other environmental assessment methods, namely the capability of rapidly screening areas with high spectral resolution instruments. This permits the identification of areas related to AMD, in this case at the S. Domingos mine, based either through waste mapping using local field spectra or on a more accurate type of mapping using a multi-source spectral methodology. Whilst the former links directly the image to the field spectra based on similarity of angular spectral distance, the latter allows the establishment of a quantitative link among multi-source data (field, standard libraries and image endmembers) that are also multi-scale spectra. This correlation matrix depicts mineralogical information to previously unknown content of field spectra and allows the elimination of uncertainty by increasing precision of the results obtained. Thus, thresholding values at ≥ 0.9 resultant from the correlation matrix of the spectra based on the wavelength values isolate a mineralogical assemblage containing copiapite and/or coquimbite closely associated with alunite. This mineralogical assemblage indicates a pH <3 environment and highlights acidic dams and ore pathway. When not isolated this class follows spatially the jarosite indicating a slightly higher pH environment, whilst goethtite-jarosite-lepidocrocite-schwertmannite is mostly confined to the village associated with waste materials dispersion. The class goethite-lepidocrocite-schwertmannite seems connected with a more geological stable framework on outcrops N of the open pit. The use of this methodology is a contribution for validation issues concerning the high precision that can be achieved by IS data, and diminishing uncertainty of the mapped areas using multi-source spectra. Thus, this methodology can be an integral part of an environmental assessment system.

Acknowledgements

The data acquisition and generation of part of the products has been collected in the framework of the MINEO project in the 5th FP (IST-1999-10337) of European Commission. We are grateful to Dr. Hartmut Mollat from BGR, responsible for the field spectroradiometric measurements as well as for his suggestions, during data capture. Post MINEO developments were partially funded through Foundation for Science and Technology of Portugal (Grant BD/17257/2004). The article has been improved by the suggestions of an anonymous reviewer and Pedro Pina.

Published with the approval of the Executive Director, British Geological Survey.

References

Abreu, M. M., Tavares, M. T., Joaquim, C., 2001. Projecto MINEO. Resultados Laboratoriais e de Campo. Instituto Superior de Agronomia. *Rel. Int. IGM*, **5**.

Abreu, M. M., Tavares, M. T., Batista, M. J., 2008. Potential use of Erica andevalensis and Erica australis in phytoremediation of sulphide mine environments: São Domingos, Portugal. *Journal of Geochemical Exploration*, **96**, 210-222.

Abreu, M. M., Batista M. J., Magalhães M. C., Matos, J. X., 2010. Acid Mine Drainage in the Portuguese Iberian Pyrite Belt. In Brock C. Robinson (Ed.) *Mine drainage and Related problems.* Nova Science Publishers, Inc. NY, **70**.

Aspinall, R. J., Marcus, W. A., Boardman, J., 2002. Considerations in collecting, processing, and analyzing high spatial resolution, hyperspectral data for environmental investigations. *Journal of Geographical Systems*, **4**, 15–29.

Boardman, J. W., 1998. Post-ATREM polishing of AVIRIS apparent reflectance data using EFFORT: a lesson in accuracy versus precision. *Proceedings of AVIRIS 1998*, JPL, California.

Boardman, J. W., Kruse, F. A., 1994. Automated spectral analysis: a geological example using AVIRIS data, north Grapevine Mountains, Nevada. *Proceedings of ERIM Tenth Thematic Conference on Geologic Remote Sensing*, Environmental Research Institute of Michigan, Ann Arbor, MI, **I**, 407-418.

Boardman, J. W., Kruse, F. A., Green, R. O., 1995. Mapping target signatures via partial unmixing of AVIRIS data. Summaries, 5th JPL Airborne Earth Science Workshop, *JPL Publication*, **95**, 1:23-26.

Clark, R. N., 1999. Spectroscopy of Rocks and Minerals, and Principles of Spectroscopy. In: Rencz, A.N. (Ed.) *Manual of Remote Sensing, V3, Remote Sensing for the Earth Sciences.* John Wiley and Sons, New York, 3-58.

Clark, R. N., Swayze, G. A., Gallagher, A. J., King, T. V., Calvin, W. M., 1993. The U. S. Geological Survey, Digital Spectral Library, Version 1: 0.2 to 3.0 microns, *U.S. Geological Survey Open File Report* 93-592, 1340.

Clark, R. N., Swayze, G. A., Wise, R., Livo, E., Hoefen, T., Kokaly, R., Sutley, S. J., 2007. USGS digital spectral library splib06a. U.S. Geological Survey, Digital Data Series 231, http://speclab.cr.usgs.gov/spectral.lib06.

Congalton, R., 2005. Thematic and Positional Accuracy Assessment of Digital Remotely Sensed Data. *Proceedings of 7th Annual Forest Inventory and Analysis Symposium*, 149-155.

Congalton, R. G., Green, K., 2009. Assessing the accuracy of remotely sensed data: Principles and practice. Boca Raton: CRC Press/Taylor and Francis, 183.

Cottard, F., 2001. S. Domingos Mine waste map. In App.2 of the MINEO Southern environment test site. *Contamination/impact mapping and modeling (2002), final report for European Comission*, 131.

Cocks T., Jenssen R., Stewart, A., Wilson, I., Shields, T., 1998. The HyMap Airborne Hyperspectral Sensor: The System, Calibration and Performance. In: Schaepman, M., Schläpfer, D., Itten, K.I. (Eds.) *Proceedings of 1st EARSeL Workshop on Imaging Spectroscopy*, Zurich, EARSeL, Paris, 37-43.

Crowley, J. K., Williams, D. E., Hammarstrom, J. M., Piatak, N., Ming Chou, I., Mars, J. C., 2003. Spectral reflectance properties (0.4–2.5 μm) of secondary Fe-oxide, Fe-hydroxide, and Fe-sulphate-hydrate minerals associated with sulphide-bearing mine wastes. *Geochemistry: Exploration, Environment, Analysis,* **3,** 3, 219-228.

Dalton, J. B., King, T. V., Bove, D. J., Kokaly, R. F., Clark, R. N., Swayze, G. A., 1998. Mapping of acid-generating and acid buffering minerals in the Animas watershed by AVIRIS spectroscopy. *Proceedings of 7th AVIRIS Earth Sci. Workshop, JPL*, **4**, 97-21.

Ferreira da Silva, E., Bobos, I., Matos, J. X., Patinha C., Reis, A. P., Cardoso Fonseca, E., 2009. Mineralogy and geochemistry of trace metals and REE in volcanic massive sulfide host rocks, stream sediments, stream waters and acid mine drainage from the Lousal mine area (Iberian Pyrite Belt, Portugal). *Applied Geochemistry*, **24**, 383-401.

Foody, G., 2008. Harshness in image classification accuracy assessment. *International Journal of Remote Sensing*, **29**, 11, 3137-3158.

Gao, B. C., Hiedebrecht, K. B., Goetz, A. F. H., 1999. Atmosphere Removal Program. *(ATREM) User's Guide version 3.1*, 101.

Goetz, A. F. H., Boardman, J. W., Kindeland, B., Heidebrecht, K. B., 1997. Atmospheric corrections: on deriving surface reflectance from hyperspectral imagers. *Proceedings SPIE*, **3118**, 14-22.

Goetz, A. F. H., Heidebrecht, K., Boardman, J. W., Kindel, B., 1998. Using ground spectral irradiance for model correction of AVIRIS data. *Summaries of the 7th Annual JPL Airborne Geoscience Workshop*, Pasadena, CA.

Green, A. A., Berman, M., Switzer, P, Craig, M. D., 1988. A transformation for ordering multispectral data in terms of image quality with implications for noise removal. *IEEE Transactions on Geoscience and Remote Sensing*, **26**, 1, 65-74.

Hammarstrom, J. M., Seal II, R. R, Meier, A. L, Kornfeld, J. M., 2005. Secondary sulfate minerals associated with acid drainage in the eastern US: recycling of metals and acidity in surficial environments. *Chemical Geology*, **215**, 407-431.

ITT, 2010. Envi Users Guide: Version 4.8. *ITT Visual Information Solutions*.

Jacquez, M., Marcus, W. A., Aspinall, R. J., Greiling, D. A., 2002. Exposure assessment using high spatial resolution hyperspectral (HSRH) imagery. *Journal of Geographical Systems*, **4**, 1, 1-14.

Kemper, T., Sommer, S., 2003. Mapping and monitoring of residual heavy metal contamination and acidification risk after the Aznalcóllar mining accident (Andalusia, Spain) using field and airborne hyperspectral data. In: Habermeyer, M., Müller, A., Holzwarth, S. (Eds.) *Proceedings of 3rd EARSEL Imaging Spectroscopy*, Herrsching, Germany, CD-ROM ISBN 2-908885-56-5, 333-343.

Kruse, F. A., Lefkoff, A. B., Boardman, J. B., Heidebrecht, K. B., Shapiro, A. T., Barloon, P. J., Goetz, A. F. H., 1993. The Spectral Image Processing System (SIPS) - Interactive Visualization and Analysis of Imaging spectrometer Data. *Remote Sensing of Environment*, **44**, 145-163.

Kruse F., Boardman, J., Huntington, J., 2003. Comparison of airborne hyperspectral data and EO-1 Hyperion for mineral mapping. *IEEE Transactions on Geoscience and Remote Sensing*, **41**, 6, 1388-1400.

Levitan, D. M., Seal, R. R., Piatak, N. M., Hammarstrom, J. M., 2007. Evaluation of acid-generating potential of complex mine wastes. *Geological Society of America, Abstracts with Programs*, **39**, 6, 404.

Mateus, A., Pinto, A., Alves, L. C., Matos, J. X., Figueiras, J., Neng, N. R., 2011. Roman and modern slag at S. Domingos mine (IPB, Portugal): compositional features and implications for their long-term stability and potential reuse. *International Journal of Environment and Waste Management*, **8**, 1-2, 133-159.

Matos, J. X., 2004. Carta geológico-mineira de São Domingos, esc. 1/5000. *Instituto Geológico e Mineiro*, Lisboa, Portugal.

Matos, J. X., Martins, L., 2006. Reabilitação ambiental de áreas mineiras do sector português da Faixa Piritosa Ibérica: estado da arte e perspectivas futuras IGME, *Bol. Geológico y Minero*, España, **117**, 289-304.

Montero, I., 2002. Multi-platform VIS/SWIR hyperspectral approach to the study of acid mine drainage from small abandoned mines. Denver Annual Meeting, Session 242. *Remotely Sensed Data for Geologic and Environmental Studies*, 242-12.

Montero, I., Brimhall, G., Alpers, C., Swayze, G., 2005. Characterization of waste rocks associated with acid drainage at the Penn Mine, California, by ground-based visible to short-wave infrared reflectance spectroscopy assisted by digital mapping. *Chemical Geology*, **215**, 453-472.

Ong, C., Cudahy, T. J., Swayze, G., 2003. Predicting Acid Drainage Related Physicochemical Measurements Using Hyperspectral Data. *Proceedings of 3rd EARSel Workshop on Imaging Spectroscopy*, Herrsching, 363-373.

Quental, L., Bourguignon, A., Batista, M. J., Brito G., Abreu, M. M., Vairinho, M., Sousa, A. J., Cottard, F., 2002a. *MINEO Southern environment test site. Contamination/impact mapping and modelling – Final report for European Comission*, 131.

Quental, L., Abreu, M. M, Oliveira, V., Sousa, P., Batista, M. J., Brito, G., Vairinho, M., Sousa, J., Martins, L., 2002b. Imagens Hiperespectrais para avaliação e monitorização ambiental em áreas mineiras: resultados preliminares do projecto Mineo na Mina de São Domingos, Alentejo. In: Brandão, J. (Ed.) *Actas do Congresso Internacional sobre Património Geológico e Mineiro*. Museu do Instituto Geológico e Mineiro, Lisboa, 583-595.

Quental, L., Brito, G., 2002c. MINEO SÃO DOMINGOS AMD waste material map (SPECTRAL ANGLE MAPPER). In Ap. 6.1-6.2 of the *MINEO Southern environment test site. Contamination/impact mapping and modeling (2002a), final report for European Comission*, 131.

Quental, L., Bourguignon, A., Cottard, F., Brito, M. G., Abreu, M. M., Sousa, A. J. Vairinho, M., 2003. Use of airborne hyperspectral Imagery for contamination mapping at São Domingos Mine, Iberian Pyrite Belt, southeast Portugal. *Proceedings of 4th European Congress on Regional Geoscientific Cartography and Information Systems*, **II**, 698-699.

Quental, L., Sousa, A. J., Marsh, S., 2011. Low pH detection in SPECIM EAGLE-HAWK using field spectra at S. Domingos Mine, SE Portugal: preliminary results. *Proceedings of 3rd Workshop on Hyperspectral Image and Signal Processing (WHISPERS): Evolution in Remote Sensing Lisbon*, Portugal, **4**.

Riaza, A., Müller, A., 2009. Hyperspectral remote sensing monitoring of pyrite mine wastes: a record of climate variability (Pyrite Belt, Spain), *Environmental Earth Sciences*, **61**, 575-594.

Riaza, A., Ong, C., Müller, A., 2007. Pyrite mine wastes hyperspectral monitoring as a tool to detect Climate Change, Proceedings of 10th Intl. Symposium on Physical Measurements and Signatures in Remote Sensing, ISPMSRS07, WG VII/1, Davos, Switzerland, 228-233.

Richards J. A., 1999. Remote Sensing Digital Image Analysis, Springer-Verlag, Berlin, 240.

Richter, N., Staenz, K., Kaufmann, H., 2008. Spectral unmixing of airborne hyperspectral data for baseline mapping of mine tailings areas. *International Journal of Remote Sensing*, **29**, 13, 3937-3956.

Schaepman, M. E., Green, R. O., Ungar, S., Boardman, J., Plaza, A. J., Gao, B. C., Ustin, S., Miller, J., Jacquemoud, S., Ben-Dor, E., Clark, R., Davis, C., Dozier, J., Goodenough, D., Roberts, D., Goetz, A. F. H., 2006. The future of imaging spectroscopy - Prospective technologies and applications. *Proceedings of IEEE International Geoscience and Remote Sensing Symposium*. Denver: IEEE, 2005-2008.

Schaepman, M., Ustin, M., Plaza, A., Painter, T., Verrelst, J., Liang, S., 2009. Earth system science related imaging spectroscopy - An assessment. *Remote Sensing of Environment*, **113**, S123–S137.

Silva, T., Figueiredo, M. O., 2010. Secondary iron sulphates in AMD: a minerochemical analysis on jarosite supporting the valorization of its geoenvironmental contribution. V. 12, EGU2010-8973, EGU General Assembly 2010.

Sousa, P., Sousa, A. J., 2000. Sistema ANDAD, CVRM - Centro de Geosistemas, IST, Lisbon.

Swayze, G. A., Clark, R. N., Pearson, R. M., Livo, K. E., 1996. Mapping Acid-Generating Minerals at the California Gulch Superfund Site in Leadville, Colorado Using Imaging Spectroscopy. *Proceedings of 6th AVIRIS Airborne Geoscience workshop*, http://popo.jpl.nasa.gov/docs/workshops/96_docs/34.PDF.

Swayze, G. A., Smith, K. S., Clark, R. N., Sutley, S. J., Pearson, R. M., Vance, J. S., Hageman, P. L., Briggs, P. H., Meier, A. L., Singleton, M. J., Roth, S., 2000. Using imaging spectroscopy to map acidic mine waste. *Environmental Science and Technology*, **34**, 47-4.

Tavares, M. T., Sousa, A. J., Abreu, M. M., 2008. Ordinary kriging and indicator kriging in the cartography of trace elements contamination in São Domingos mining site (Alentejo, Portugal). *Journal of Geochemical Exploration*, **98**, 43-56.

Tavares, M. T, Abreu, M. M, Vairinho, M. M., Sousa, A. J., Quental, L., 2009. Comportamento geoquímico de alguns elementos vestigiais na envolvente das Minas de S. Domingos, Alentejo: áreas da Tapada e do Telheiro. *Revista de Ciências Agrárias*, **32**, 1, 182-194.

Zabcic, N., Ong, C., Mueller, A., Rivard, B., 2005. Mapping Surface pH Using Airborne Hyperspectral Imagery at the Sotiel-Migollas Mine, Spain. In: Zagajewski, B., Sobczak, M., Wrzesień, M., (Eds.) *Proceedings of 4th EARSeL Workshop on Imaging Spectroscopy*. New quality in environmental studies. EARSeL and Warsaw University, Warsaw.

Zhang, Y., Desai, D., 2000. Hyperspectral image compression based on adaptive recursive bidirection prediction/JPEG[J]. *Pattern Recognition*, **33,** 1851-61.